Frontiers of Information Technology & Electronic Engineering
www.zju.edu.cn/jzus; engineering.cae.cn; www.springerlink.com
ISSN 2095-9184 (print); ISSN 2095-9230 (online)
E-mail: jzus@zju.edu.cn

A new variable-mode control strategy for LLC resonant converters operating in a wide input voltage range*

Hui-pin LIN†, Xiao-guang JIN, Liang XIE, Jin HU, Zheng-yu LU†‡
(*College of Electrical Engineering, Zhejiang University, Hangzhou 310027, China*)
†E-mail: linhuipin@126.com; eeluzy@cee.zju.edu.cn

Received Jan. 20, 2016; Revision accepted Nov. 10, 2016; Crosschecked Feb. 21, 2017

Abstract: This paper proposes a new variable-mode control strategy that is applicable for LLC resonant converters operating in a wide input voltage range. This control strategy incorporates advantages from full-bridge LLC resonant converters, half-bridge LLC resonant converters, variable-frequency control mode, and phase-shift control mode. Under this control strategy, different input voltages determine the different operating modes of the circuit. When the input voltage is very low, it works in a full-bridge circuit and variable frequency mode (FB_VF mode). When the input voltage rises to a certain level, it shifts to a full-bridge circuit and phase-shifting control mode (FB_PS mode). When the input voltage further increases, it shifts into a half-bridge circuit and variable frequency mode (HB_VF mode). Such shifts are enabled by the digital signal processor (DSP), which means that no auxiliary circuit is needed, just a modification of the software. From light load to heavy load, the primary MOSFET for the LLC resonant converter can realize zero-voltage switching (ZVS), and the secondary rectifier diode can realize zero-current switching (ZCS). With an LLC resonant converter prototype with a 300 W rated power and a 450 V output voltage, as well as a resonant converter with 20–120 V input voltage, the experiments verified the proposed control strategy. Experimental results showed that under this control strategy, the maximum converter efficiency reaches 95.7% and the range of the input voltage expands threefold.

Key words: LLC; Full bridge; Half bridge; Variable frequency; Phase shift; Wide input voltage range
http://dx.doi.org/10.1631/FITEE.1600029 **CLC number:** TM923.61

1 Introduction

Thanks to its environment-friendly characteristics, reliability, maturity, and cost efficiency, wind power is currently the fastest growing new energy technology. In 2012, China possessed an installed wind power capacity of 75 324 MW (Tian *et al*., 2014), which was the highest such capacity in the world. Moreover, a 200 GW capacity in 2020 is expected (Wang *et al*., 2013). The wind power is distributed in a wide area; however, it is distributed unevenly and changes seasonally. In light of this, the development of wind power shows a polarized trend: (1) Large wind power plants adopt a high-capacity grid-connected wind power turbine. (2) In these distributed power generation systems (Song, *et al*., 2003), small- and medium-sized wind power turbines prevail. Along with China's economic development, an increasing number of small- and medium-sized wind power systems are used in family and business buildings, and operated in a grid-connected manner. These facts serve as the focus in Walker and Pierce (2006).

Fig. 1 shows the structure of a distributed grid-generation system (Walker and Sernia, 2004). A wind-power generation system can be divided into several or dozens of power channels. In every one of them, the permanent magnet synchronous generator (PMSG) produces electricity (Rajaei *et al*., 2013), the rectifier module rectifies the current (after

‡ Corresponding author
* Project supported by the National Natural Science Foundation of China (Nos. 51177148 and 51407151)
ORCID: Zheng-yu LU, http://orcid.org/0000-0003-1032-2938

rectification, the DC input voltage is 20–120 V), and then the DC/DC module raises the voltage to DC bus voltage (450 V). Afterwards, all the electricity in these channels gathers in a DC bus, flows through the inverter, and eventually to the grid (220 V, 50 Hz, AC, China).

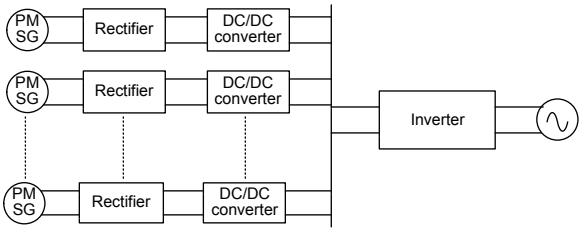

Fig. 1 Block flow diagram of a wind power system with a DC modular grid structure (PMSG: permanent magnet synchronous generator)

Fig. 1 indicates that due to the great disparity between input voltage (20–120 V) and output voltage (450 V) and the security regulations that must be taken into consideration, the circuit must be separated. Meanwhile, the challenge is in how to collect more energy within the super-wide input voltage range, i.e., keeping the maximum efficiency of the wind power generation system within that super-wide input range. In short, the DC/DC module has three features: (1) wider range, (2) separation, and (3) high efficiency. However, features (1) and (3) are generally contradictory.

As shown in Fig. 2, the load gain property of an LLC resonant converter is that the maximum gain increases with the load equivalent resistance, which is required by the wide input voltage range. Meanwhile, the LLC resonant converter features primary MOSFET zero-voltage switching (ZVS) and secondary diode zero-current switching (ZCS), which are the requirements for a wider range (Hu *et al*., 2015). Hence, the LLC resonant converter was chosen for the DC/DC module for a distributed wind power system in Jiang (2006) and Liang *et al*. (2010).

To maintain the high gain and wide input voltage range of the LLC resonant converter, the magnetic inductance value must be fairly low (Fang *et al*., 2007; Jung and Kwon, 2007; Zhang *et al*., 2009; Jang *et al*., 2012). However, the increased primary-winding MOSFET conduction loss and core loss reduce the efficiency of the LLC resonant converter (Steigerwald, 1988; Chen *et al*., 2010; Fang *et al*., 2012).

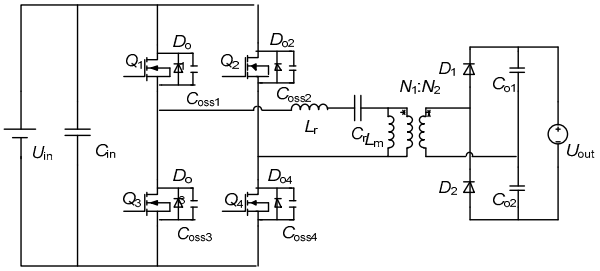

Fig. 2 Full-bridge LLC resonant converter

Many studies have been conducted to find ways to cope with these problems which constantly occur in traditional LLC resonant converters, and to obtain high-efficiency generation. Liang *et al*. (2010) proposed a mixed control strategy (Fig. 2), which doubled the DC gain by changing the full bridge into a half bridge. Nonetheless, the input voltage range of the actual wind power generation is wider; hence, such a strategy is inapplicable.

Yang *et al*. (2003) put forward another solution (Fig. 3) where according to the level of the input voltage, the transformation ratio was altered by shifting the secondary windings (W_1 and W_2). The problem with this structure is that it is too complex: compared to a traditional LLC resonant converter, it has one more secondary winding, two more diodes, and one more MOSFET. In other words, the circuit loss is increased, and the circuit design is difficult.

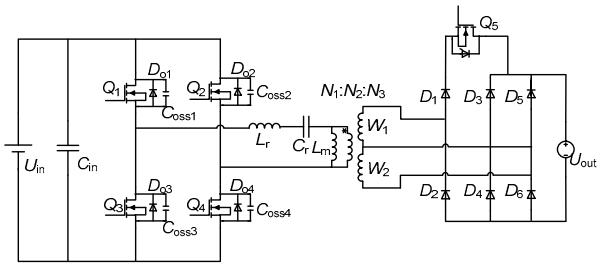

Fig. 3 LLC resonant converters with a double-secondary transformer

To overcome the shortcomings of a traditional LLC resonant converter, this paper adopts a variable-mode control strategy to gain higher efficiency for a wider range. In the so-called variable-mode control strategy, with no change in the structure of the circuit, the converter proactively controls the modes to shift it into a specific circuit formation and operating mode.

With the new variable-mode control strategy, different circuit modes can be adopted in accordance with different input voltages, and consequently, the range of input voltages can be widened, the MOSFET

operating frequency is reduced, the circuit design is facilitated, excitation loss and circuit loss are decreased, and efficiency is maximized.

2 Principles of variable-mode control strategy

Fig. 2 demonstrates the main circuit and MOSFETs of the full-bridge LLC resonant converter; Q_1–Q_4 are the inverter bridge arms. The diodes D_{o1}–D_{o4} are parasitic diodes of Q_1–Q_4, and C_{oss1}–C_{oss4} are parasitic capacitances of Q_1–Q_4. In the circuit for the primary winding of the transformer, the resonant capacitance C_r, resonant inductor L_r, and magnetic inductance L_m form a resonant tank. In the circuit for the secondary winding of the transformer, the diodes D_1 and D_2, and the output capacitances C_{o1} and C_{o2}, form a voltage-doubling rectifier.

The variable-mode control strategy is composed of three operating modes as follows:

Mode 1: As shown in Fig. 4a, when the input voltage U_{in} is lower than a certain threshold U_{th1}, the circuit adopts a full-bridge LLC topology, and the converter works in variable-frequency mode. The circuit works at this moment in the mode of a traditional LLC resonant converter (Fig. 5a shows its main working waves), called 'FB_VF mode'.

Mode 2: As shown in Fig. 4b, when the input voltage is higher than the threshold value U_{th1} but lower than the threshold U_{th2}, the circuit adopts a full-bridge LLC topology, and the converter works in phase-shifting mode (Hamamura *et al*., 2003; Lin *et al*., 2013). Its main operating waveform is presented in Fig. 5b. The driving signal for Q_1–Q_4 here is the square signal with a 50% duty ratio, and Q_1–Q_4 are in phase-shifting control. At this point, Q_1 and Q_3 are the leading legs, and Q_2 and Q_4 are the lagging legs. The mode is called 'FB_PS mode'.

Mode 3: As shown in Fig. 4c, when the input voltage is higher than the threshold U_{th2} so that Q_2 stays off while Q_4 stays on, Q_1 and Q_3 are in variable-frequency control, and turn-ons and turn-offs are alternatively performed by the square signal with a 50% duty ratio. At this moment, the circuit shifts to a half-bridge LLC topology and the converter works in variable-frequency mode. With this mode, the DC gain is only half of that with Mode 1 under the same working conditions. The operating waveform here is similar to Mode 1, called 'HB_VF mode'.

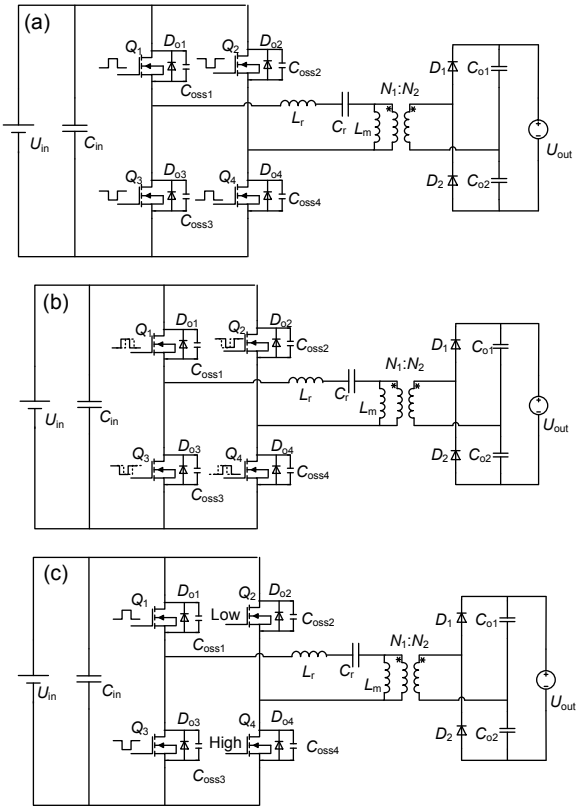

Fig. 4 Different operating modes: (a) Mode 1; (b) Mode 2; (c) Mode 3

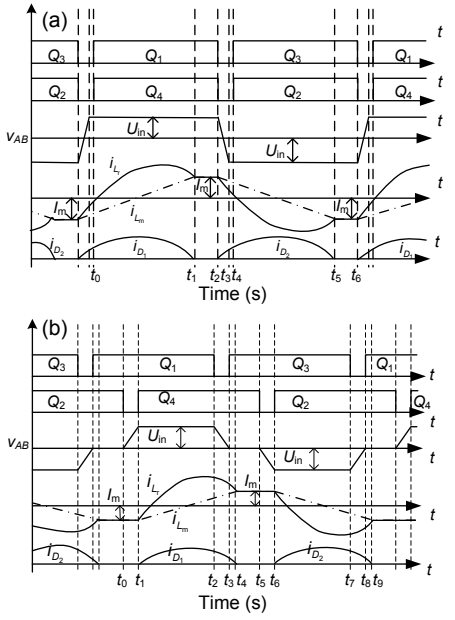

Fig. 5 Main waveforms of the LLC resonant converter in FB_VF mode (a) and FB_PS mode (b)

The principles of Mode 1 and Mode 3 were described in Liang *et al*. (2010). Hence, in this study we analyze only Mode 2 (FB_PS mode) through examples, and suppose that the working frequency here is equal to or slightly higher than the resonant frequency.

1. In switch mode 0 (before t_0) (Fig. 6a), before time t_0, Q_1 and Q_2 are on, Q_3 and Q_4 are off, L_r, C_r, and L_m resonate together. In the primary and secondary windings of the transformer flows there is no electronic current, and the converter load is powered by the output capacitances C_{o1} and C_{o2}.

2. In switch mode 1 (t_0–t_1) (Fig. 6b), Q_2 is turned off at time t_0: due to the buffering of the parasitic capacitances C_{oss2} and C_{oss4}, Q_2 could be turned off with zero voltage. Since this period is fairly short, it could likewise be considered that both the resonant current i_{L_r} and the magnetizing current i_{L_m} remain unchanged; thus, the converter load is still powered by the output capacitances C_{o1} and C_{o2}.

3. In switch mode 2 (t_1–t_2) (Fig. 6c), at time t_1, the voltage of C_{oss2} rises to U_{in} while that of C_{oss4} is reduced to 0; the inverse-parallel diode D_{o4} is on, and hence Q_4 could realize ZVS. At this moment, the voltages between points A and B are equal (u_{AB}=U_{in}), the rectifier diode D_1 turns on, the primary winding voltage is kept at nU_{out}, and the magnetizing current i_{L_m} increases linearly.

4. In switch mode 3 (t_2–t_3) (Fig. 6d), Q_1 is turned off at time t_2. Due to the buffering of C_{oss1}, Q_1 is turned on with zero voltage. The rectifier diode D_1 is on, nU_{out} is added on L_m, and the magnetizing current i_{L_m} increases linearly.

5. In switch mode 4 (t_3–t_4) (Fig. 6e), at time t_3, the voltage of C_{oss1} rises to U_{in} while that of C_{oss4} is reduced to 0, the inverse-parallel diode D_{o4} is on, and hence Q_3 could realize ZVS. By this time, u_{AB}=0, the voltage of the transformer's primary winding is still clamped at nU_{out}, and i_{L_m} increases linearly. L_r and C_r resonate together.

6. In switch mode 5 (t_4–t_5) (Fig. 6f), at time t_4, i_{L_r} equals i_{L_m}, and the primary winding current i_{L_p} of the transformer is reduced to 0; the current in rectifier diode D_1 naturally free-wheels to 0, and hence it can be turned off with zero voltage without a problem

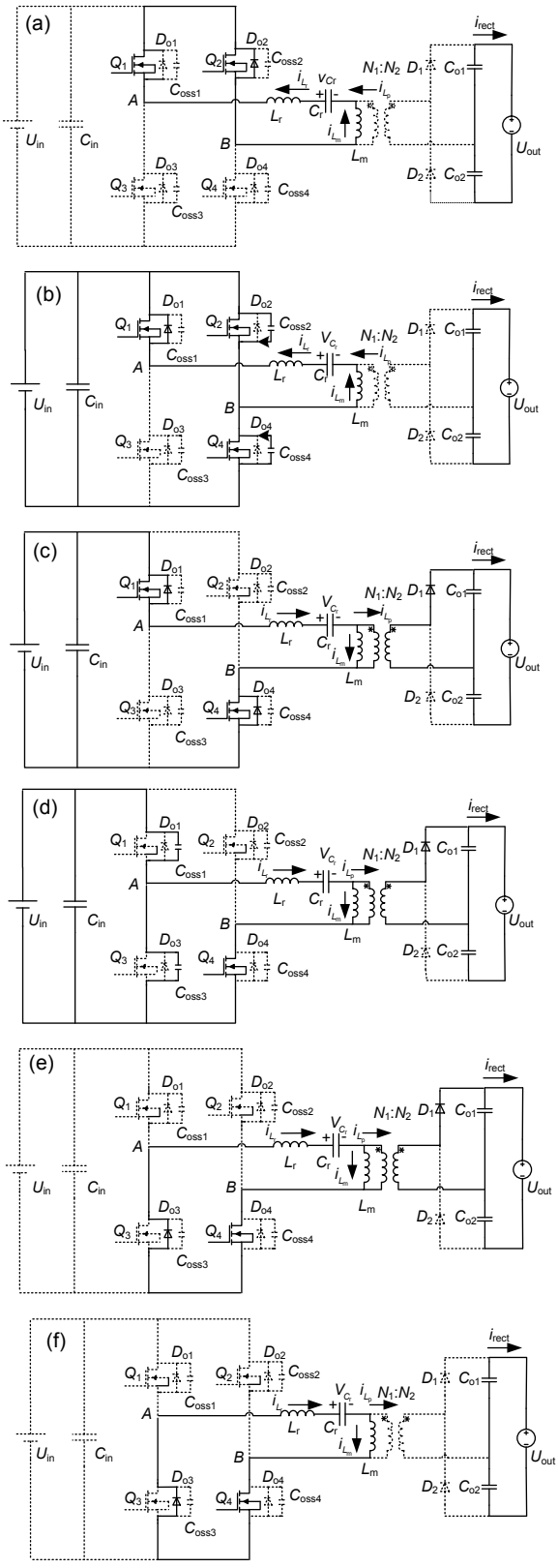

Fig. 6 Equivalent circuits in FB_PS mode stages: (a) before t_0; (b) t_0–t_1; (c) t_1–t_2; (d) t_2–t_3; (e) t_3–t_4; (f) t_4–t_5

with reverse recovery. Load is powered by output capacitances C_{o1} and C_{o2}. In this period, L_r and L_m are connected in series and resonate with C_r.

At time t_5, Q_4 is turned off with zero voltage and another half operating period begins based on similar principles, which do not need to be repeated here.

Analyses of the working states and waveforms above indicate that zero-voltage switching of the primary winding MOSFET and zero-current switching of the secondary winding diode are realized on the circuit in FB_PS mode.

3 Gain analysis of the LLC resonant converter in different modes

The resonant tank for the LLC resonant converter can be drawn similarly to the circuit diagram in Fig. 7, where $R_{eq}=(8/\pi^2)n^2R_o$ ($n=N_1/N_2$) is the load resistance converted to the primary winding.

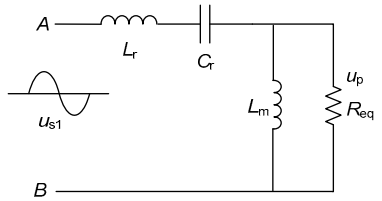

Fig. 7 A simplified equivalent circuit diagram of the LLC resonant converter resonant tank

From Fig. 7, the AC gain of the resonant tank is found to be approximate to

$$G(k_f,h,Q)=|u_p/u_{s1}| =\left[\left(1+\frac{1}{h}-\frac{1}{k_f\cdot h^2}\right)^2+Q^2\cdot\left(k_f-\frac{1}{k_f}\right)^2\right]^{-\frac{1}{2}}, \tag{1}$$

where u_p denotes the RMS of the fundamental wave of the primary winding voltage's square wave, u_{s1} denotes the RMS of the fundamental wave of the resonant tank's input voltage, $Q=Z_m/R_{eq}$ denotes the quality factor, $h=L_m/L_r$ is the inductance ratio, $k_f=f/f_r$ is the normalized frequency, f is the operating frequency, $f_r=1/(2\pi\sqrt{L_rC_r})$ is the series resonant frequency, and $Z_0=\sqrt{L_r/C_r}$ is the characteristic impedance.

As shown in Fig. 2, the output segment of the converter is the voltage-doubling rectifier. Thus, it is calculated to the secondary winding of the transformer, $R_o=U_{out}^2/(4P_{out})$, where U_{out}, which is a fixed constant, is the DC bus voltage that the resonant converter inputs into the inverter (the DC bus is directly connected with the inverter), and P_{out}, which changes with the working conditions, denotes the capacity of the grid-connected inverter. Hence, it can be concluded that the quality factor Q is a one-variable function of P_{out}. Assuming that the parameters of the LLC circuit are fixed, h and n are also constants.

Thus, the DC gain of the LLC resonant converter could approximately be expressed as

$$M(k_f,P_{out})=U_{out}^2/U_{in}. \tag{2}$$

3.1 FB_VF mode

When the input voltage U_{in} is lower than the threshold U_{th1}, and the main circuit is in FB_VF mode, we have $u_{s1}=\sqrt{2}U_{in}/\pi$, while $u_p=\sqrt{2}nU_{out}/(2\pi)$, so the DC voltage gain could approximately be expressed as

$$M_{FB\_VF}(k_f,P_{out})=\frac{U_{out}}{U_{in}}=\frac{2}{n}G(k_f,h,Q) =\frac{2}{n}\left[\left(1+\frac{1}{h}-\frac{1}{k_f\cdot h^2}\right)^2+\left(\frac{\pi^2P_{out}}{2n^2U_{out}^2}\sqrt{\frac{L_r}{C_r}}\right)^2 \cdot\left(k_f-\frac{1}{k_f}\right)^2\right]^{-\frac{1}{2}}. \tag{3}$$

It can be derived from Eq. (3) that the voltage transfer ratio M_{FB_VF} is a function of k_f and P_{out}, and the 3D curves of M_{FB_VF} with respect to k_f and P_{out} are shown in Fig. 8.

3.2 FB_PS mode

When the input voltage is higher than the threshold U_{th1}, and lower than threshold U_{th2}, the converter is in FB_PS mode. Fig. 9 provides the driving waveforms of Q_1–Q_4, denoting a half period as π. τ ($0\le\tau\le\pi$) is the phase shifting angle, $u_{s1}=\sqrt{2}U_{in}\sin[(\pi-\tau)/2]/\pi$, and $u_p=\sqrt{2}nU_{out}/(2\pi)$.

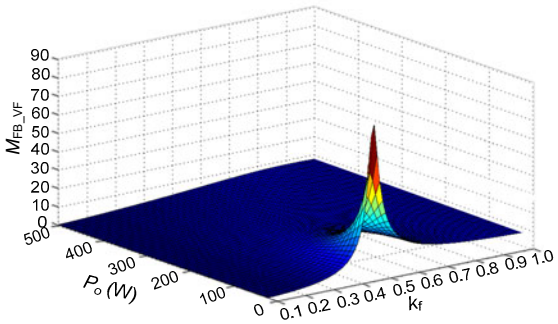

Fig. 8 Three-dimensional curves of M_{FB_VF} gain in FB_VF mode

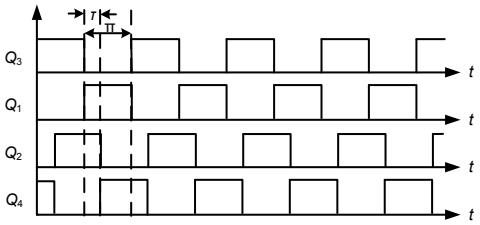

Fig. 9 Driving waveforms in FB_PS mode

During phase-shifting control, the converter operates around the resonant frequency; thus, the DC gain can approximately be expressed as

$$M_{FB\_PS}(k_f, P_{out}, \tau) = \frac{U_{out}}{U_{in}} = \frac{2\sin[(\pi-\tau)/2]}{n} G(k_f, h, Q)$$
$$= \frac{2\sin[(\pi-\tau)/2]}{n} \left[\left(1+\frac{1}{h}-\frac{1}{k_f \cdot h^2}\right)^2 + \left(\frac{\pi^2 P_{out}}{2n^2 U_{out}^2}\sqrt{\frac{L_r}{C_r}}\right)^2 \cdot \left(k_f - \frac{1}{k_f}\right)^2 \right]^{-\frac{1}{2}}, \quad 0 \le \tau \le \pi. \tag{4}$$

From Eq. (4) it can be derived that the voltage gain ratio M_{FB_PS} is a function of k_f, P_{out}, and τ. When the output power P_{out} and the frequency k_f stay unchanged, the gain will decrease with the rise of the phase shifting angle. Meanwhile, when the output power P_{out} and the phase shifting angle τ stay unchanged, the gain is reduced with the increase in frequency. When P_{out}=300 W, the 3D curves of M_{FB_PS} with respect to k_f and τ are shown in Fig. 10.

3.3 HB_VF mode

When the input voltage is higher than the threshold U_{th2}, the circuit is in HB_VF mode. As shown in Fig. 7, the input voltage u_{s1} of the RMS of the resonant tank in HB_VF mode is half of that in FB_VF mode, where $u_{s1} = \sqrt{2}U_{in}/(2\pi)$. While $u_p = \sqrt{2}nU_{out}/(2\pi)$, the DC gain in FB-VF mode is half of that in HB_VF mode, so the DC voltage gain could approximately be expressed as

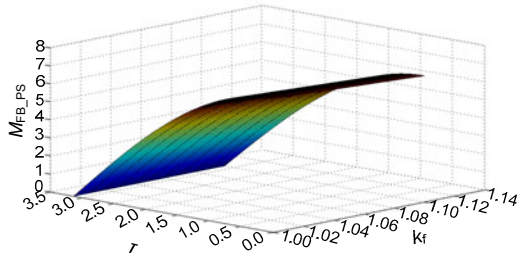

Fig. 10 Three-dimensional curves for M_{FB_PS} gain in FB_PS mode

$$M_{HB\_VF}(k_f, P_{out}) = \frac{U_{out}}{U_{in}} = \frac{1}{n} G(k_f, h, Q)$$
$$= \frac{1}{2} M_{FB\_VF}(k_f, P_{out})$$
$$= \frac{1}{n} \left[\left(1+\frac{1}{h}-\frac{1}{k_f \cdot h^2}\right)^2 + \left(\frac{\pi^2 P_{out}}{2n^2 U_{out}^2}\sqrt{\frac{L_r}{C_r}}\right)^2 \cdot \left(k_f - \frac{1}{k_f}\right)^2 \right]^{-\frac{1}{2}}. \tag{5}$$

It can be derived from Eq. (5) that the voltage gain ratio M_{HB_VF} is a function of k_f and P_{out}, and the 3D curves of M_{HB_VF} with respect to k_f and P_{out} are shown in Fig. 11.

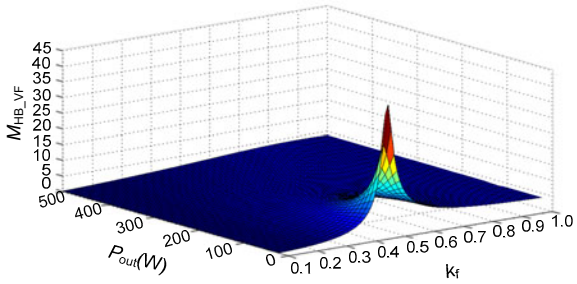

Fig. 11 Three-dimensional curves of the M_{HB_VF} gain in FB_VF mode

When the circuit works in HB_VF mode or FB_VF mode, the working frequency f is normally subject to $f_m < f \le f_r$, where $f_m = \left(2\pi\sqrt{(L_r + L_m)C_r}\right)^{-1}$ is another resonant frequency. If $f \ge f_r$, the ZCS of the secondary winding diode cannot be realized, and

hence the efficiency drops. When $f \geq f_r$, the circuit works in FB_PS mode, the aforementioned problem can consequently be addressed, the input voltage range can be expanded, and a zero-current turn-off of the secondary winding diode can be realized.

4 Parameter compatibility design for the variable-mode LLC resonant converter

The rated power equals P_{out}. Segment the circuit into three voltage sections. Presume that the operating voltage range in Mode 1 (FB_VF mode) is U_{min1}–U_{max1} (Fig. 12), the circuit works under the maximum power point track (MPPT), and the output power rises with voltage. In Mode 2 (FB_PS mode), the input voltage range is U_{min2}–U_{max2} and the output power remains P_{out}. In Mode 3 (HB_VF mode), the input voltage range is U_{min3}–U_{max3} and the output power remains P_{out}.

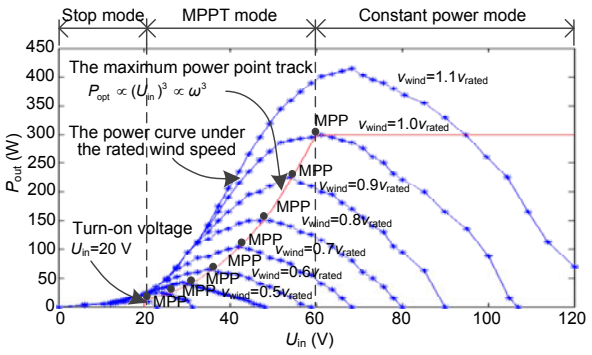

Fig. 12 Relationship between wind power turbine output voltage and output power

4.1 Determination of the transformer turns ratio

When the voltage is within U_{min2}–U_{max2} or U_{min3}–U_{max3}, the output power P_{out} remains unchanged. Here, the corresponding voltage of the rated power P_{out} is U_{max2}, and U_{max2}=U_{min3}, with the resonance frequency f_r, and the dead time denoted as T_{dead}.

It is suggested that the voltage ratio between the primary and secondary sides of the transformer is

$$n = \frac{U_{out}/2}{U_{max2}}. \tag{6}$$

Thus, the transformer ratio is obtained.

4.2 Calculation of magnetizing inductance L_m, resonant inductor L_r, and resonant capacitor C_r

In total, there are two conditions for ZVS on the primary side of the LLC resonant converter:

1. The current angle is greater than the dead angle. The dead angle refers to the product of dead time and the switch cycle angular frequency. The physical significance of a current angle greater than the dead angle lies in how the current on the resonant inductor during dead time cannot be reversed, ensuring that the parasitic diode being driven is kept open before the arrival of the driving signal; in other words, it is a soft switching.

2. Parasitic capacitance is fully charged or discharged during the dead time.

In Mode 1 (FB_VF mode) (Fig. 12), the input voltage range is U_{min1}–U_{max1}, and the output power P_{out} is in direct proportion to the third power of the input voltage. Then, the minimal critical value of the current angle is θ_{cri}=$2\pi f_r \cdot T_{dead}$, and the output power is $P_{out} = kU_{in}^3 = k'f_s^3$, where k and k' are constants. When the dead time is fixed, the realization of ZVS depends mainly on the magnetizing inductance L_m, operating frequency f_s, and output current I_o (with the output voltage U_{out} unchanged).

Based on the condition $\theta_{cri} = 2\pi f_r \cdot T_{dead}$ and the current angle $\theta \geq \theta_{cri}$, we have

$$L_m \leq \frac{n^2 U_{out}/2}{2\pi f_r (2I_o)\tan(2\pi f_r T_{dead})} \cdot \frac{f_s}{f_r}. \tag{7}$$

Since the output voltage U_{out} does not change, we have I_o=P_{out}/U_{out}, and the output power is P_{out}=$kU_{in}^3 = k'f_s^3$, and $L_m \leq \frac{n^2 U_{out}^2}{8\pi f_r \tan(2\pi f_r T_d)\cdot k'f_s^2} \cdot \frac{1}{f_r}$. It is suggested that when operating frequency f_s grows, $\frac{n^2 U_{out}^2}{8\pi f_r \tan(2\pi f_r T_d)\cdot k'f_s^2} \cdot \frac{1}{f_r}$ is reduced. Here, when the operating frequency f_s is at a maximum, i.e., f_s=f_r, the minimum value of L_m can be obtained. This satisfies the ZVS condition of a primary MOSFET under the entire input voltage range of Mode 1 (FB_VF mode).

In Mode 2 (FB_PS mode) (Fig. 12), the input voltage range is U_{min2}–U_{max2}, the power is P_{out},

$L_m \le \frac{n^2 U_{out}/2}{2\pi f_r (2I_o)\tan(2\pi f_r T_d)} \cdot \frac{f_s}{f_r}$, and the operating frequency rises with input voltage. Thus, as long as f_s=f_r, L_m is kept at a minimum value. Similar results can be found for Mode 3 (HB_VF mode).

Thus, when f_s=f_r, L_m meets the ZVS conditions in a full range.

When the fully resonant point is set in advance, there are countless combinations of resonant inductor L_r and resonant capacitor C_r. We need to satisfy the requirements of fixed gain at the lowest operating frequency and L_r and C_r in conformity with the sum of the relevant output power. By using a fundamental harmonic approximation (FHA), the model can be built and the parameters are designed effectively.

In Mode 1 (FB_VF mode), the operating frequency is below the resonance frequency f_r. From Fig. 12 it can be seen that the output power P_{out} is in direct proportion to the third power of the input voltage U_{in}, and $P_{out} = kU_{in}^3$.

Thus, the gain curve of the LLC resonant converter is found: when U_{in}=U_{min1}, the required gain, at maximum, is U_{out}/U_{min1}. Then, from the point of minimum input voltage, find the resonant inductor that satisfies the requirements for the maximum gain under the lowest frequency. Let the operating frequency under such a minimum input voltage be half of the resonance frequency.

When f_s=1/2f_r, i.e., k_f=1/2, the equation can be written as

$$M_{FB\_VF}(k_f, P_{out}) = M_{FB\_VF}\left(\frac{1}{2}, kU_{min1}^3\right) \ge \frac{U_{out}}{U_{min1}}. \quad (8)$$

In Mode 2 (FB_PS mode), the converter works above the resonance frequency f_r, the input voltage U_{in} grows, and the output power P_{out} remains unchanged. The converter here works under the conditions of fixed frequency and shifting phase, and the voltage is affected by both frequency and the duty ratio. When U_{in}=U_{min2}, the required gain is U_{out}/U_{min2} at maximum, where the operating frequency is f_r (i.e., k_f=1), the phase-shifting angle is 0, and the expression is

$$M_{FB\_PS}(k_f, P_{out}, \tau) = M_{FB\_PS}(1, P_{out}, 0) \ge \frac{U_{out}}{U_{min2}}. \quad (9)$$

In Mode 3 (HB_VF mode), the converter works under resonance frequency f_r again, the input voltage U_{in} increases, and the output power P_{out} remains unchanged. Thus, the gain curve of the LLC resonant converter is found here. When U_{in}=U_{min3}, the required gain, to the maximum, is U_{out}/U_{min3}. Let the minimum operating frequency in Mode 3 be $k_{HB\_VF\_min}$. We have

$$M_{HB\_VF}(k_f, P_{out}) = M_{HB\_VF}(k_{HB\_VF\_min}, P_{out}) \ge \frac{U_{out}}{U_{min3}}. \quad (10)$$

When Eqs. (14)–(16) are satisfied, the optimized resonant inductor L_r and resonant capacitor C_r can be chosen.

To maintain the continuity of the input voltage change, we must keep the voltage gains between the mode shifting points at equality, i.e., U_{max1}=U_{min2}, U_{max2}=U_{min3}.

4.3 Criteria for selecting the voltage threshold between different modes

The common operating frequency f_s of the LLC resonant converter is subject to f_s≤f_r, which is the condition under which the operation in Mode 1 (FB_VF mode) is conducted.

When the operating frequency is f_s>f_r, the secondary diode of the transformer cannot be turned off with zero current (ZCS), resulting in lower efficiency. When the circuit works around the fully resonant point, f_s is slightly larger than f_r. Let T_s≈T_r and the converter works in Mode 2 (FB_PS mode).

A working analysis suggests that the LLC converter with PWM control can satisfy the circuit gain (enlarge the input voltage range) and meanwhile evade the problem that the secondary diode of the transformer cannot be turned off with zero current, thus having the shortcoming of frequency control in the region f_s>f_r under Mode 1. Specifically, the diode hard turn-off problem is accounted for.

In Mode 2 (FB_PS mode), the gain of LLC is reduced with the duty ratio. When the phase-shifting angle grows, however, the magnetic inductor is clamped in a shorter time, the current at the intersection of resonance current and the magnetic current decreases, and thus it is harder to turn on the lagging leg with zero voltage.

While the duty ratio is changed, the features for pulse-frequency modulation (PFM) control are

retained and the gain reduces with the growth in frequency.

As depicted in Fig. 7, the input impedance of the resonant tank is given by

$$Z_{\text{in}}=\frac{1-\omega^2 L_{\text{r}}C_{\text{r}}}{\text{j}\omega C_{\text{r}}}+\frac{\text{j}\omega L_{\text{m}}R_{\text{eq}}}{R_{\text{eq}}+\text{j}\omega L_{\text{m}}}, \tag{11}$$

where $\omega=2\pi f_{\text{s}}$.

In Mode 2 (FB_PS mode), the circuit represents the structure of the full-bridge resonant tank, and the current can be described as $I_{\text{r\_mode2}}=U_{\text{in}}/Z_{\text{in}}$.

In Mode 3 (HB_VF mode), it is a half-bridge structure, and the equivalent input voltage is also a half of the full-bridge structure. Therefore, under the same operating frequency, the resonance current of Mode 3 (HB_VF mode) is also a half of that of Mode 2 (FB_PS mode), $I_{\text{r\_mode3}}=U_{\text{in}}/(2Z_{\text{in}})$.

From the shifting points equations between Mode 2 and Mode 3 in Table 1, we have

$$\begin{cases}\dfrac{U_{\text{min3}}}{Z_{\text{in}}}=\dfrac{U_{\text{max2}}}{2Z_{\text{in}}},\\ M_{\text{FB\_PS}}=M_{\text{HB\_VF}}=\dfrac{U_{\text{min3}}}{U_{\text{out}}}=\dfrac{U_{\text{max2}}}{U_{\text{out}}}.\end{cases} \tag{12}$$

Table 1 Mode shifting conditions

Shifting type	Shifting point
From Mode 1 to Mode 2	$f_{\text{s}}=f_{\text{r}}$
From Mode 2 to Mode 3	$I_{\text{r\_mode2}}=I_{\text{r\_mode3}}$ $M_{\text{FB\_PS}}=M_{\text{HB\_VF}}$

The curves are shown in Fig. 13, which gives $|1/Z_{\text{in}}|$, $|1/(2Z_{\text{in}})|$, and the operating frequency. Therefore, through comparing the resonant tank currents

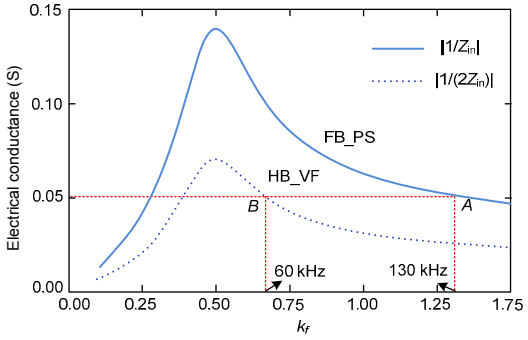

Fig. 13 Comparison of resonant tank currents before and after mode shifting

with the same input voltage and observing Eq. (12) and Fig. 13, for the voltage between the modes we have $U_{\text{th1}}=U_{\text{max1}}=U_{\text{min2}}$ and $U_{\text{th2}}=U_{\text{max2}}=U_{\text{min3}}$.

Shifting from FB_PS mode to HB_VF mode (point *A* to *B*), it can be observed from Fig. 13 that when the gain $U_{\text{out}}/U_{\text{in}}$ remains unchanged, the resonant tank current remains unchanged as well, and the operating frequency is reduced. As a result, the circuit works under $f_{\text{s}}\le f_{\text{r}}$, the best condition, and vice versa.

5 Confirmation of circuit parameters and analysis of the modes

Based on the analysis and requirements presented above, we have the following calculations for the parameter design. Table 2 gives the known parameters calculated in Section 4.

Table 2 Working parameters for the resonant converter and the parameters of other components

Item	Value
Input voltage U_{in}	20–120 V
Output power U_{out}	450 V
Rated power P_{out}	300 W
Resonant frequency f_{r}	100 kHz
Resonant capacitor C_{r}	200 nF
Resonant inductor L_{r}	12.5 μH
Excitation inductance L_{m}	45 μH
MOSFET Q_1–Q_4	IPP65R310CFD
Rectifying diodes D_1–D_2	MUR8100
Ratio of transformer N_1:N_2	8:30

The input voltage range of the LLC converter is 20–120 V. At different input voltage levels, the converter works in a different mode.

According to the known conditions in Table 3, and with the method in Section 4.3, the voltage threshold can be calculated as $U_{\text{th1}}=U_{\text{max1}}=U_{\text{min2}}=60$ V and $U_{\text{th2}}=U_{\text{max2}}=U_{\text{min3}}=80$ V.

Table 3 Relationship between the operating modes and input voltage

Input voltage (V)	Operating mode	DC gain
20–60	FB_VF	22.500–7.500
60–80	FB_PS	7.500–5.625
80–120	HB_VF	5.625–3.750

It can be derived from Table 3 that when the input voltage range U_{in} is 20–60 V, the output voltage

U_{out} is 450 V, DC gain M_{FB_VF} is 22.500–7.500, and the converter works in FB_VF mode. Fig. 12 indicates that when U_{in} is 20–60 V, the generator works on a maximum power tracking curve, as shown in Fig. 14, and the converter must work on the red curve among the 3D curves. As shown in Fig. 14, the working frequency and DC gain increase with an increase in the tracked power, where the tracking power P_{out} and input voltage U_{in} are in a third-order relationship.

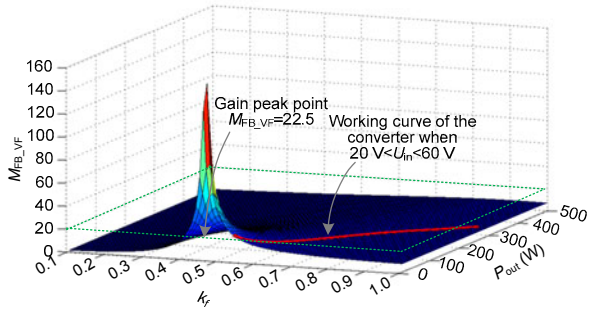

Fig. 14 Working curves of the converter in FB_VF mode (20 V<U_{in}<60 V) (References to color refer to the online version of this figure)

It can be derived from Table 1 that when the input voltage range U_{in} is 60–80 V, the DC gain M_{FB_PS} is 7.500–5.625, and the converter works in FB_PS mode. As shown in Fig. 12, when U_{in} is between 60 V and 80 V, the generator works in constant power mode, and P_{out}=300 W. From Fig. 15 it can be derived that when P_{out}=300 W and the phase shifting angle τ stays unchanged, the gain M_{FB_PS} drops with the reduction in phase shifting angle τ; furthermore, the M_{FB_PS} gain drops with the decrease in working frequency k_f.

Theoretically, when the working frequency is the resonant frequency, the DC gain from 7.500 to 5.625 could be realized through a raise in the phase shifting angle τ. The larger the phase shifting angle, however, the shorter the time for the excitation inductance to be voltage clamped, the smaller the current at the intersection point of the resonant current and magnetizing current, and the harder it is to realize the ZCS on the lagging bridge legs. Meanwhile, the resonant current rises, and the reactive power loss of the resonant tank grows. For these reasons, in FB_PS mode, it is not recommended that the gain be obtained just by increasing the phase shifting angle. When the angle is too wide, ZVS cannot be realized, the circuit working efficiency is reduced, and a capacitive resonant tank might occur, which leads to a short circuit on the bridge arms and causes damage.

Here is the solution. Since the M_{FB_PS} gain drops with an increase in working frequency k_f, when the working frequency rises, the phase shifting angle τ could be reduced, which shortens the time for the resonant current circulation and enhances the converter efficiency. From Fig. 15, it can be derived that when the range of the input voltage U_{in} is 60–80V, the working area can be divided into several parts. In each part's control area, by fixing the frequency, the gain is reduced with the increase in the phase shifting angle. When it comes to the next part, as the working frequency increases, the phase shifting angle drops at first and then rises. By doing this, the phase shifting angle τ in each part will not be too large, which ensures the ZCS of a secondary winding diode and the ZVS of a primary MOSFET.

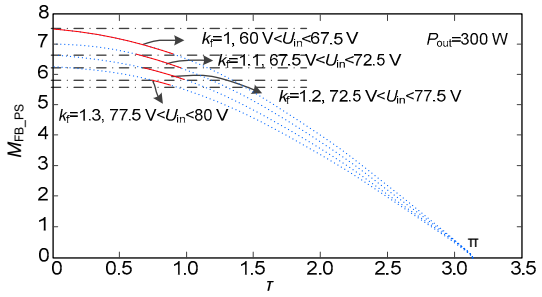

Fig. 15 Working curves for the converter in FB_PS mode (60 V<U_{in}<80 V)

It can be derived from Table 2 that when the input voltage range U_{in} is 80–120 V, the DC gain M_{FB_PS} is 7.5–5.625, and the converter works in HB_VF mode. As shown in Fig. 12, when U_{in} is between 80 and 120 V, the turbine works in constant power mode, and P_{out}=300 W. From Fig. 16 it can be derived that when P_{out}=300 W, the M_{HB_VF} gain drops with a decrease in the working frequency k_f.

In Fig. 17, line *AB* represents the frequency-gain curve of FB_VF mode. From *A* to *B*, the output power is also increasing. Line *CD* represents the phase shifting-gain curve, and the direction of the arrow indicates the direction along which the operating frequency increases. Fig. 17 shows that points *B* and *C* coincide. It means that the change of gain and control amount is continuous when shifting from FB_VF mode to FB_PS mode. When the input voltage is subject to U_{in}>U_{th1}=60 V, as described in Table 1, the operating frequency f_s=f_r; when it is shifted to

FB_PS mode, the operating frequency remains unchanged. The phase-shifting angle τ grows gradually as the voltage increases, until reaching the stable status. In contrast, when the input voltage is $U_{in}<U_{th1}=60$ V as described in Table 1 and the LLC is shifted to FB_VF mode, the phase-shifting angle is reduced gradually to zero as the voltage decreases, and the switch frequency decreases and remains stable at $f_s=f_r$.

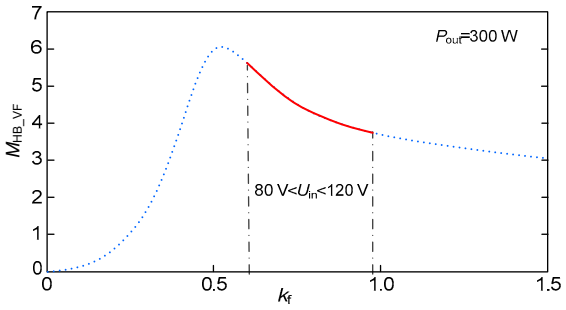

Fig. 16 Working curves for the converter in HB_VF mode (80 V<U_{in}<120 V)

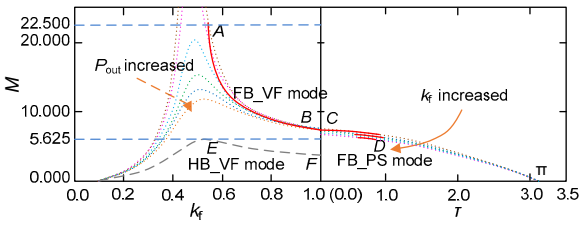

Fig. 17 Voltage gain variation curves for switching among three modes

In Fig. 17, line *EF* represents the frequency-gain curve of HB_VF mode. From *E* to *F*, the output power remains unchanged. Fig. 17 shows that the operating frequency f_s and the phase-shifting angle τ of points *E* and *F* are very different. It means that the change in the control amount is discontinuous when shifting from FB_PS to HB_VF. When the input voltage $U_{in}>U_{th2}=80$ V, the LLC is shifted to HB_VF mode (shifted from *D* to *E*), the phase-shifting angle is reduced to 0, and the operating frequency decreases. When the input voltage $U_{in}<U_{th2}=80$ V, the LLC is shifted to FB_PS mode (shifted from *E* to *F*), the phase-shifting angle grows, and the switch frequency augments to $f_s=1.3f_r$.

6 Experimental verification

Fig. 18a presents waveforms of the resonant current, gate-source voltage U_{gs} of MOSFET Q_3, drain-source voltage U_{ds}, and output voltage U_{out}. When the LLC resonant converter works in FB_VF mode, the input voltage $U_{in}=25$ V and output power $P_{out}=25$ W. From Fig. 18b it can be seen that when the circuit works in FB_VF mode and with a light load on the primary winding MOSFET, ZVS can easily be realized.

Fig. 19a presents waveforms for the resonant current, gate-source voltage U_{gs} of MOSFET Q_3, drain-source voltage U_{ds}, and output voltage U_{out}. When the LLC resonant converter works in FB_PS mode, the input voltage $U_{in}=65$ V and output power $P_{out}=300$ W. From Fig. 19b it can be seen that when the circuit works in FB_PS mode and with a full load on the primary MOSFET, ZVS can also be realized easily.

Fig. 20a presents waveforms of resonant current, gate-source voltage U_{gs} of MOSFET Q_3, drain-source voltage U_{ds}, and output voltage U_{out}. When the LLC resonant converter works in FB_VF mode, the input voltage $U_{in}=90$ V and output power $P_{out}=300$ W. From Fig. 20b it can be seen that when the circuit works in FB_VF mode and with a full load on the primary winding MOSFET, the zero-voltage start can also easily be realized.

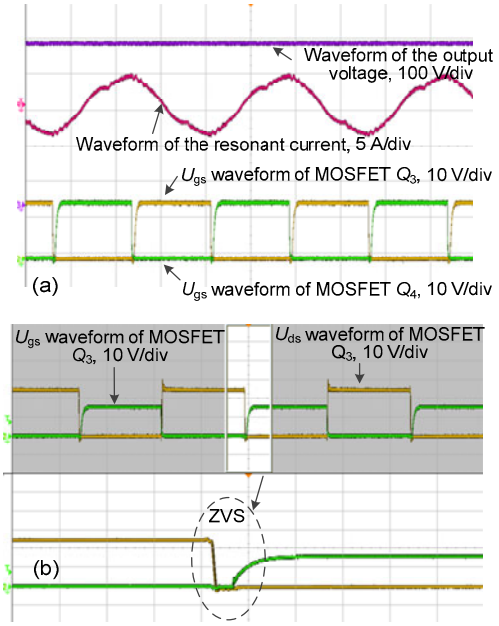

Fig. 18 FB_VF mode of the LLC resonant converter: (a) waveforms of the resonant current and output voltage; (b) waveforms of U_{gs} and U_{ds} of the primary winding MOSFET (testing conditions: $U_{in}=25$ V, $U_o=450$ V, and $P_{out}=25$ W)

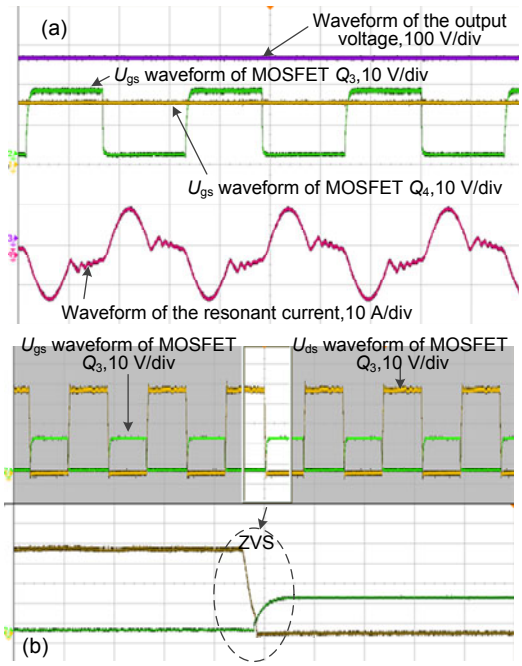

Fig. 19 FB_PS mode of the LLC resonant converter: (a) waveforms of resonant current and output voltage; (b) waveforms of U_{gs} and U_{ds} of the primary winding MOSFET (testing conditions: U_{in}=65 V, U_o=450 V, and P_{out}=300 W)

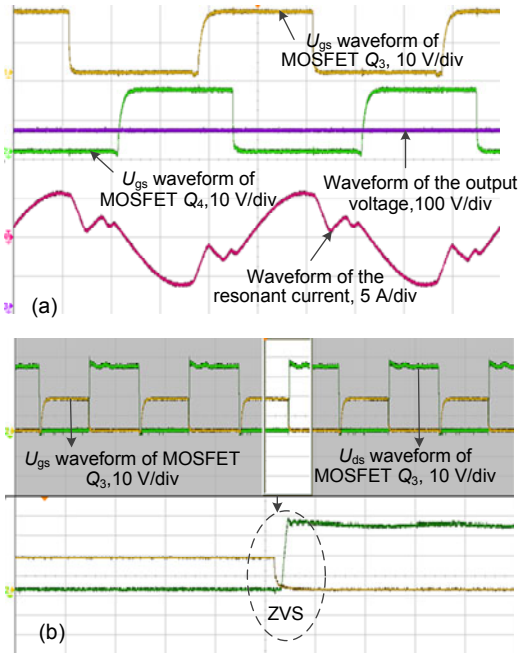

Fig. 20 HB_VF mode of the LLC resonant converter: (a) waveforms of resonant current and output voltage; (b) waveforms of U_{gs} and U_{ds} of the primary winding MOSFET (testing conditions: U_{in}=90 V, U_o=450 V, and P_{out}=300 W)

Fig. 21 presents the working efficiency curves of a resonant converter under the traditional full-bridge LLC strategy and the variable-mode control strategy. As shown in Fig. 21, the converter under the variable-mode control strategy has a 2% higher efficiency than the traditional one. Under the variable-mode control strategy, the maximum working efficiency can reach 95.7%.

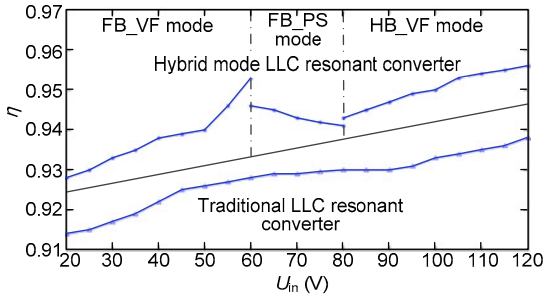

Fig. 21 Efficiency curves for a resonant converter under traditional and the variable-mode strategies

7 Conclusions

Due to fluctuations in wind speed, wind power generation systems often face extremely wide input voltage ranges in the DC module. Given these circumstances, we proposed a new control strategy that enables the LLC resonant converter to work within an ultra-wide voltage range. When the input voltage is fairly low, an FB_VF mode is adopted; when it rises to a certain extent, a full-bridge phase shifting mode (FB_PS mode) is adopted; when it keeps rising, a half-bridge variable frequency mode (HB_VF mode) is employed. By shifting between a half bridge and a full bridge, the input voltage range can be doubled. Furthermore, in the full-bridge phase shifting mode, the input voltage range can increase further. After experimental verification, it has been proven that the converter using the variable-mode control strategy has a higher efficiency than that using traditional strategies.

References

Chen, W., Hong, X.Y., Wang, S.R., *et al*., 2010. High efficiency soft-switched step-up DC-DC converter with hybrid mode LLC+C resonant tank. 25th Annual IEEE Applied Power Electronics Conf. and Exposition, p.1358-1364. http://dx.doi.org/10.1109/APEC.2010.5433406

Fang, X., Hu, H.B., Shen, J., *et al*., 2012. An optimal design of the LLC resonant converter based on peak gain estimation. 27th Annual IEEE Applied Power Electronics Conf. and Exposition, p.1286-1291. http://dx.doi.org/10.1109/APEC.2012.6165984

Fang, Y., Xu, D.H., Zhang, Y.J., *et al*., 2007. Design of high power density LLC resonant converter with extra wide input range. 22nd Annual IEEE Applied Power Electronics Conf., p.976-981. http://dx.doi.org/10.1109/APEX.2007.357633

Hamamura, S., Ninomiya, T., Yamamoto, M., *et al*., 2003. Combined PWM and PFM control for universal line voltage of a piezoelectric transformer off-line converter. *IEEE Trans. Power Electron.*, **18**(1):270-277. http://dx.doi.org/10.1109/TPEL.2002.807177

Hu, J., Lin, H.P., Lu, Z.Y., *et al*., 2015. Flexible resonant tank for a combined converter to achieve an HPS and LED compatible driver. *Front. Inform. Technol. Electron. Eng.*, **16**(8):679-693. http://dx.doi.org/10.1631/FITEE.1500054

Jang, J., Joung, M., Choi, B., *et al*., 2012. Dynamic analysis and control design of optocoupler-isolated LLC series resonant converters with wide input and load variations. *IET Power Electron.*, **5**(6):755-764. http://dx.doi.org/10.1049/iet-pel.2011.0289

Jiang, Z.H., 2006. Power management of hybrid photovoltaic—fuel cell power systems. IEEE Power Engineering Society General Meeting, p.3458-3463. http://dx.doi.org/10.1109/PES.2006.1709000

Jung, J.H., Kwon, J.G., 2007. Theoretical analysis and optimal design of LLC resonant converter. European Conf. on Power Electronics and Applications, p.1134-1143. http://dx.doi.org/10.1109/EPE.2007.4417639

Liang, Z.G., Guo, R., Wang, G.Y., *et al*., 2010. A new wide input range high efficiency photovoltaic inverter. IEEE Energy Conversion Congress and Exposition, p.2937-2943. http://dx.doi.org/10.1109/ECCE.2010.5618217

Lin, B.R., Nian, Y.B., Shiau, T.Y., 2013. Resonant converter with fixed frequency control. IEEE Region 10 Conf. TENCON, p.1-6. http://dx.doi.org/10.1109/TENCON.2013.6718908

Rajaei, A., Mohamadian, M., Varjani, A.Y., 2013. Vienna-rectifier-based direct torque control of PMSG for wind energy application. *IEEE Trans. Ind. Electron.*, **60**(7):2919-2929. http://dx.doi.org/10.1109/TIE.2012.2227905

Steigerwald, R.L., 1988. A comparison of half-bridge resonant converter topologies. *IEEE Trans. Power Electron.*, **3**(2):174-182. http://dx.doi.org/10.1109/63.4347

Song, S.H., Kang, S.I., Hahm, N.K., 2003. Implementation and control of grid connected AC-DC-AC power converter for variable speed wind energy conversion systems. 18th Annual IEEE Applied Power Electronics Conf. and Exposition, p.154-158. http://dx.doi.org/10.1109/APEC.2003.1179207

Tian, J., Su, C., Soltani, M., *et al*., 2014. Active power dispatch method for a wind farm central controller considering wake effect. 40th Annual Conf. of the IEEE Industrial Electronics Society, IECON, p.5450-5456. http://dx.doi.org/10.1109/IECON.2014.7049333

Walker, G.R., Pierce, J.C., 2006. PhotoVoltaic DC-DC module integrated converter for novel cascaded and bypass grid connection topologies—design and optimisation. 37th IEEE Power Electronics Specialists Conf. Records, p.1767-1773. http://dx.doi.org/10.1109/PESC.2006.1712242

Walker, G.R., Sernia, P.C., 2004. Cascaded DC-DC converter connection of photovoltaic modules. *IEEE Trans. Power Electron.*, **19**(4):1130-1139. http://dx.doi.org/10.1109/TPEL.2004.830090

Wang, C.X., Lu, Z.X., Qiao, Y., 2013. A consideration of the wind power benefits in day-ahead scheduling of wind-coal intensive power systems. *IEEE Trans. Power Syst.*, **28**(1):236-245. http://dx.doi.org/10.1109/TPWRS.2012.2205280

Yang, B., 2003. Topology Investigation of Front End DC/DC Converter for Distributed Power System. PhD Thesis, Virginia Polytechnic Institute and State University, Blacksburg, USA.

Zhang, Z., Thomsen, O.C., Andersen, M.A.E., 2009. A DC-DC converter with wide input voltage range for fuel cell and supercapacitor application. Int. Conf. on Power Electronics and Drive Systems, p.1324-1329. http://dx.doi.org/10.1109/PEDS.2009.5385904